

# ELEMENTAL ABUNDANCES OF BLUE COMPACT DWARFS FROM MID-IR SPECTROSCOPY WITH SPITZER

YANLING WU<sup>1</sup>, J. BERNARD-SALAS<sup>1</sup>, V. CHARMANDARIS<sup>2,3</sup>, V. LEBOUTEILLER<sup>1</sup>, LEI HAO<sup>1</sup>, B. R. BRANDL<sup>4</sup>, J. R. HOUCK<sup>1</sup>

*Accepted by ApJ, September 28th, 2007*

## ABSTRACT

We present a study of elemental abundances in a sample of thirteen Blue Compact Dwarf (BCD) galaxies, using the  $\sim 10\text{--}37\mu\text{m}$  high resolution spectra obtained with Spitzer/IRS. We derive the abundances of neon and sulfur for our sample using the infrared fine-structure lines probing regions which may be obscured by dust in the optical and compare our results with similar infrared studies of starburst galaxies from ISO. We find a good correlation between the neon and sulfur abundances, though sulfur is under-abundant relative to neon with respect to the solar value. A comparison of the elemental abundances (neon, sulfur) measured from the infrared data with those derived from the optical (neon, sulfur, oxygen) studies reveals a good overall agreement for sulfur, while the infrared derived neon abundances are slightly higher than the optical values. This indicates that either the metallicities of dust enshrouded regions in BCDs are similar to the optically accessible regions, or that if they are different they do not contribute substantially to the total infrared emission of the host galaxy.

*Subject headings:* dust, extinction — galaxies:starburst — abundances

## 1. INTRODUCTION

Blue Compact Dwarf Galaxies (BCDs) are dwarf galaxies with blue optical colors resulting from one or more intense bursts of star-formation, low luminosities ( $M_B > -18$ ) and small sizes. The first BCD discovered was I Zw 18 by Zwicky (1966), which had the lowest oxygen abundance observed in a galaxy (Searle & Sargent 1972), until the recent study of the western component of SBS0335-052 (Izotov et al. 2005). Although BCDs are defined mostly by their morphological parameters, they are globally found to have low heavy element abundances as measured from their HII regions ( $1/30 Z_\odot \sim 1/2 Z_\odot$ ). The low metallicity of BCDs is suggestive of a young age since their interstellar medium is chemically unevolved. However, some BCDs do display an older stellar population and have formed a large fraction of their stars more than 1 Gyr ago (see Loose & Thuan 1985; Aloisi et al. 2007). The plausible scenario that BCDs are young is intriguing within the context of Cold Dark Matter models which predict that low-mass dwarf galaxies, originating from density perturbations much less massive than those producing the larger structures, can still be forming at the current epoch. However, despite the great success in detecting galaxies at high redshift over the past few years, bona fide young galaxies still remain extremely difficult to find in the local universe (Kunth & Sargent 1986; Kunth & Östlin 2000; Madden et al. 2006). This is likely due to the observational bias of sampling mostly luminous more evolved galaxies at high redshifts. If some BCDs are truly young galaxies, they would provide an

ideal local laboratory to understand the galaxy formation processes in the early universe.

Over the past two decades, BCDs have been studied extensively in many wavelengths using ground-based and space-born instruments (for a review see Kunth & Östlin 2000). In the FUV, the Far Ultraviolet Spectroscopic Explorer (FUSE) has been used to study the chemical abundances in the neutral gas in several BCDs (Thuan et al. 2002; Aloisi et al. 2003; Lebouteiller et al. 2004). Optical spectra have been obtained for a large number of BCDs and display strong narrow emission lines resulting from the intensive star-formation processes that take place in these systems (Izotov et al. 1997; Izotov & Thuan 1999b; Pustilnik et al. 2005; Salzer et al. 2005). The Infrared Space Observatory (ISO) revealed unexpectedly that despite their low metallicities, BCDs, such as SBS0335-052E, could still have copious emission from dust grains (Thuan et al. 1999; Madden 2000; Madden et al. 2006; Plante & Sauvage 2002). More recently, the Spitzer Space Telescope (Werner et al. 2004) has been used to observe these metal-poor dwarf systems in order to study their dust continuum properties and the polycyclic aromatic hydrocarbon (PAH) features (Houck et al. 2004b; Hogg et al. 2005; Engelbracht et al. 2005; Rosenberg et al. 2006; Wu et al. 2006; O'Halloran et al. 2006; Hunt et al. 2006; Wu et al. 2007). Finally, radio observations have also been performed for several BCDs to study their HI kinematics and distribution (Thuan et al. 2004) and thermal/non-thermal continuum emission properties (Hunt et al. 2005).

Metallicity is a key parameter that influences the formation and evolution of both stars and galaxies. Detailed studies of the elemental abundances of BCDs have already been carried out by several groups (Izotov & Thuan 1999b; Kniazev et al. 2003; Shi et al. 2005) and the well known metallicity-luminosity relation

Electronic address: wyl@astro.cornell.edu, jbs@isc.astro.cornell.edu, vassiliadis@physics.uoc.gr, vianney@isc.astro.cornell.edu, hao@astro.cornell.edu, brandl@astro.cornell.edu

<sup>1</sup> Astronomy Department, Cornell University, Ithaca, NY 14853

<sup>2</sup> University of Crete, Department of Physics, GR-71003, Heraklion, Greece

<sup>3</sup> IESL/Foundation for Research and Technology - Hellas, GR-71110, Heraklion, Greece and Chercheur Associé, Observatoire de Paris, F-75014, Paris, France

<sup>4</sup> Leiden Observatory, Leiden University, P.O. Box 9513, 2300 RA Leiden, The Netherlands

TABLE 1  
OBSERVING PARAMETERS OF THE SAMPLE

Object Name	RA (J2000)	Dec (J2000)	AORKEY	Observation Date	Redshift	On-source Time (Sec) SH LR
Haro11	00h36m52.5s	-33d33m19s	9007104	2004-07-17	0.0206	480 240
NGC1140	02h54m33.6s	-10d01m40s	4830976	2004-01-07	0.0050	480 240
SBS0335-052E	03h37m44.0s	-05d02m40s	11769856	2004-09-01	0.0135	1440 960
NGC1569	04h30m47.0s	+64d50m59s	9001984	2004-03-01	$\sim 0$	480 240
IIZw40	05h55m42.6s	+03d23m32s	9007616	2004-03-01	0.0026	480 240
UGC4274	08h13m13.0s	+45d59m39s	12076032	2004-10-23	0.0015	120 56
			12626688	2004-11-11		120 56
I Zw18	09h34m02.0s	+55d14m28s	9008640	2004-03-27	0.0025	480 240
			16205568	2005-12-16		2880 1440
VIIZw403	11h27m59.9s	+78d59m39s	9005824	2004-12-09	$\sim 0$	480 240
Mrk1450	11h38m35.6s	+57d52m27s	9011712	2004-12-12	0.0032	480 240
UM461	11h51m33.3s	-02d22m22s	9006336	2005-01-03	0.0035	480 240
			16204032	2006-01-14		1440 ...
SBS1210+537A	12h12m55.9s	+53d27m38s	8989952	2004-06-06	...	480 240
Tol1214-277	12h17m17.1s	-28d02m33s	9008128	2004-06-28	0.0260	480 240
Tol65	12h25m46.9s	-36d14m01s	4829696	2004-01-07	0.0090	480 240
UGCA292	12h38m40.0s	+32d46m01s	4831232	2004-01-07	0.0010	480 240
Tol1304-353	13h07m37.5s	-35d38m19s	9006848	2004-06-25	0.0140	480 240
Pox186	13h25m48.6s	-11d37m38s	9007360	2004-07-14	0.0039	480 240
CG0563	14h52m05.7s	+38d10m59s	8992512	2005-05-30	0.0324	240 120
CG0598	14h59m20.6s	+42d16m10s	8992256	2005-03-19	0.0575	480 240
CG0752	15h31m21.3s	+47d01m24s	8991744	2005-03-19	0.0211	480 240
Mrk1499	16h35m21.1s	+52d12m53s	9011456	2004-06-05	0.0090	480 240
[RC2]A2228-00	22h30m33.9s	-00d07m35s	9006080	2004-06-24	0.0052	480 240

NOTE. — The coordinates and redshifts of the objects are cited from the NASA/IPAC Extragalactic Database (NED). In this paper, we only include the analysis of thirteen out of twenty-two sources which have SNRs sufficient for our abundance study. CG0563, CG0598 and CG0752 are included in the original sample as BCD candidates, however, they appear to be more starburst like (see Hao et al. 2007). Thus even though they have high SNR, we do not include these three sources in this study.

has also been studied in detail in the environment of dwarf galaxies (Skillman et al. 1989; Hunter & Hoffman 1999; Melbourne & Salzer 2002). However, because these studies were performed in the optical, they were limited by the fact that the properties of some of the deeply obscured regions in the star-forming galaxies may remain inaccessible due to dust extinction at these wavelengths. In fact, Thuan et al. (1999), using ISO, have shown that the eastern component of SBS 0335-052 does have an embedded super star cluster (SSC) that is invisible in the optical while contributing  $\sim 75\%$  to the bolometric luminosity (see also Plante & Sauvage 2002; Houck et al. 2004b), even though it has very low metallicity ( $12+\log(\text{O}/\text{H})=7.33$ ), which would in principle imply a low dust content. In addition to probing the dust enshrouded regions, emission in the infrared also has the advantage that the lines accessible at these wavelengths are less sensitive to the electron temperature fluctuations than the corresponding optical lines of the same ion. In the infrared, more ionization stages of an element become available as well. The improved sensitivity of the Infrared Spectrograph (IRS<sup>5</sup>) (Houck et al. 2004a) on Spitzer has enabled us to obtain for the first time infrared spectra for a much larger sample of BCDs than was previously possible (Thuan et al. 1999; Madden 2000; Verma et al. 2003; Martín-Hernández et al. 2006), thus motivating this study to probe the heavy element abundances in BCDs.

In this paper, we analyze Spitzer/IRS spectra of thir-

teen BCDs and present elemental abundances of neon and sulfur, which are both primary elements produced by the same massive stars in the nuclear synthesis processes. In section 2, we describe the sample selection, observations and data reduction. We present our results on the chemical abundances in section 3, followed by a comparison of the optical and infrared derived abundances in section 4. We show the interplay between the abundances and PAH emission in section 5. Finally, we summarize our conclusions in section 6.

## 2. OBSERVATIONS AND DATA REDUCTION

As part of the *IRS* Guaranteed Time Observation (GTO) program, we have compiled a large sample of BCD candidates selected from the Second Byurakan Survey (SBS), Bootes void galaxies (Kirshner et al. 1981; Popescu & Hopp 2000), and other commonly studied BCDs. Details on the low-resolution spectra of the sample have been published by Wu et al. (2006).

We acquired the targets using the red ( $22\mu\text{m}$ ) *IRS* peak-up camera in high accuracy mode to locate the mid-IR centroid of the source and then offset to the appropriate slit using the standard *IRS* staring observing mode. Subsequently, we obtained the  $10\text{--}37\mu\text{m}$  spectra for our sources using the *IRS* Short-High (SH,  $9.9\text{--}19.6\mu\text{m}$ ) and Long-high (LH,  $18.7\text{--}37.2\mu\text{m}$ ) modules. No spectra of the background were obtained. The AORkey and on-source integration time of the twenty-two sources for which we obtain high-resolution spectroscopy are given in Table 1. In this paper, we focus on the description and analysis of thirteen BCDs from our program which have a signal-to-noise ratio (SNR) high enough for our elemental abundance study.

<sup>5</sup> The IRS was a collaborative venture between Cornell University and Ball Aerospace Corporation funded by NASA through the Jet Propulsion Laboratory and the Ames Research Center.

The data were processed by the *Spitzer* Science Center (SSC) pipeline version 13.2. The three-dimensional data cubes were converted to two-dimensional slope images after linearization correction, subtraction of darks, and cosmic-ray removal. The reduction of the spectral data started from intermediate pipeline products “droop” files, which only lacked stray light and flat-field correction. Individual pointings to each nod position of the slit were co-added. The data from SH and LH were extracted using the full slit extraction method of a script version of *IRS* data analysis package SMART (Higdon et al. 2004) from the median of the combined images. The 1-dimensional spectra were flux calibrated by multiplying by a relative spectral response function (RSRF), which was created from the *IRS* standard star,  $\xi$  Dra, for which accurate templates were available (Cohen et al. 2003; Sloan et al. 2007). As a final cosmetic step the ends of each order where the noise increases significantly were manually clipped. No scaling was needed between the adjacent orders within the same module. For faint sources, the spectra taken at nod position 1 are severely affected by fringing problems, thus we only use the data at nod position 2 for these sources in our study.

The fine-structure lines, [SIV]  $\lambda 10.51\mu\text{m}$ , [NeII]  $\lambda 12.81\mu\text{m}$ , [NeIII]  $\lambda 15.55\mu\text{m}$  and [SIII]  $\lambda 18.71\mu\text{m}$ ,  $33.48\mu\text{m}$  are clearly present in the majority of the BCDs in our sample<sup>6</sup>. We measure the line fluxes by fitting them with a Gaussian profile. Even though the [SIII] line is visible in both SH and LH we only use the  $18.71\mu\text{m}$  line for deriving the ionic abundance. This is because by using lines within the same module (SH), we remove uncertainties due to the different sizes of the SH and LH slits. Furthermore, the [SIII]  $\lambda 33.48\mu\text{m}$  line is near the cut off of the LH module where the sensitivity drops dramatically, making its measurement more uncertain in some cases.

### 3. ELEMENTAL ABUNDANCES OF BCDs

In this section, we derive the neon and sulfur abundances using the new infrared data of our BCD sample. The elemental abundances of the compact HII regions in our Galaxy (Martín-Hernández et al. 2002; Simpson et al. 2004), in the Magellanic Clouds (Vermeij et al. 2002), as well as in starburst galaxies (Verma et al. 2003; Martín-Hernández et al. 2006) have already been studied extensively in the past using ISO, and more recently with *Spitzer* (Rubin et al. 2007). There are several methods to derive the chemical abundances (for a review see Stasińska 2007). Here we use an empirical method, which derives ionic abundances directly from the observed lines of the relevant ions. To do so, we need to have the flux of at least one hydrogen recombination line, the dust extinction, as well as the electron temperature and density of the interstellar medium (ISM).

#### 3.1. Electron density and temperature

The electron density ( $N_e$ ) could in principle be determined by comparing the measured ratio of [SIII]  $18.71\mu\text{m}/33.48\mu\text{m}$  to the expected theoretical value

<sup>6</sup> See Fig. 3 of Wu et al. (2006), or Hao et al. (2007) for the reduced spectra.

using the corresponding *S*-curve (see Houck et al. 1984). However, the values for the ratio are in the horizontal part of the *S*-curve and as a result we cannot use these two lines to accurately constrain the electron density of these systems. Furthermore, the  $33.48\mu\text{m}$  [SIII] line is located at the edge of the LH slit, where the sensitivity drops dramatically, and considering that these emission lines are weak, the measured line flux for the  $33.48\mu\text{m}$  [SIII] has a large uncertainty. Since the infrared determination of elemental abundances does not depend strongly on the density, we adopted the optically derived electron densities from the literature, which range from 10 to  $3000\text{cm}^{-3}$  (see Table 2). For sources where such information is not available, we adopt a typical electron density of  $100\text{cm}^{-3}$  in this paper.

Since BCDs in general have low metallicities, it is expected that BCDs would have relatively high electron temperatures ( $T_e$ ). Fortunately, the infrared lines are much less sensitive to the uncertainties in the electron temperature compared to the optical (Bernard Salas et al. 2001). As a result we adopt electron temperatures derived from the optical studies found in the literature. For sources which do not have direct measurements (which happen to be high metallicity sources in our sample, e.g. NGC1140, UGC4274), we use a representative temperature of  $T_e = 10,000\text{K}$  (see Table 2).

#### 3.2. Ionized hydrogen flux estimates

In order to derive the ionic abundances, we also need to obtain information on at least one hydrogen recombination line (usually  $\text{H}\beta$ ). For sources in which the Humphreys  $\alpha$  ( $\text{H}\alpha$ ,  $12.37\mu\text{m}$ ) line is detected, we use it to convert to  $\text{H}\beta$ . From the extinction corrected  $\text{H}\alpha$  flux, we estimate the  $\text{H}\beta$  flux using the values given in the tables of Hummer & Storey (1987) for Case B recombination. This has the advantage that we do not need to correct for aperture effects because the neon and sulfur lines we use to derive the abundances also reside in the same module (SH). The  $12.37\mu\text{m}$  line is generally very weak and it is detected in six of our thirteen sources. For SBS0335-052E and IZw18, which have radio continuum data, we calculate the  $\text{H}\beta$  flux from the thermal free-free emission using the fraction included in the aperture of our SH slit at the time of the observation, and no correction for extinction is needed. For the remaining four sources which have  $\text{H}\alpha$  images available from Gil de Paz et al. (2003), we overlay the SH slit on each  $\text{H}\alpha$  image to calculate what fraction of the  $\text{H}\alpha$  emission is included in our slit. Then we derive the corresponding  $\text{H}\beta$  flux inside the SH slit from the extinction-corrected  $\text{H}\alpha$  flux. Finally, for UM461, we use the  $\text{H}\beta$  flux of the whole galaxy from the integrated spectra (Moustakas & Kennicutt 2006). UM461 is a very compact source, thus fully encompassed within the SH slit.

#### 3.3. Extinction correction

All our measurements, both the fluxes from the  $\text{H}\alpha$  images, as well as the infrared lines, have been corrected for extinction. From the low-resolution spectra of our BCDs (Wu et al. 2006), we find that most of the sources do not show a strong  $9.7\mu\text{m}$  silicate feature, thus indicating an intrinsically relatively low dust extinction. Due to the

TABLE 2  
OPTICAL PROPERTIES OF THE SOURCES

Object	F(H $\beta$ ) ( $\times 10^{-14}$ ergs s $^{-1}$ cm $^{-2}$ )				$E_{B-V}$ mag	$T_e$ K	$N_e$ cm $^{-3}$	ref
	Hu $\alpha$ -derived	H $\alpha$ -derived	radio-derived	optical				
Haro11	252 $\pm$ 40	...	...	...	0.41	13700	10	(1)
NGC1140	67 $\pm$ 9	...	...	...	0.10	10000	100	(2) <sup>a</sup>
SBS0335-052E	<22.4	...	6.5 $\pm$ 0.06	...	2.76	20000	200	(3),(4),(5)
NGC1569	393 $\pm$ 19	...	...	...	0.65	12000	100	(6)
II Zw40	363 $\pm$ 10	282 $\pm$ 22	...	...	0.79	13000	190	(2),(7)
UGC4274	<59.6	11.5 $\pm$ 1.0	...	...	0	10000	62	(7),(8) <sup>a</sup>
IZw18	<12.6	8.0 $\pm$ 0.6	6.1 $\pm$ 0.6	...	0.08	19000	100	(7),(9),(10)
VI Zw403	<24.6	11.8 $\pm$ 1.2	...	...	0	14800	100	(7),(11)
Mrk1450	<14.8	15.8 $\pm$ 1.4	...	...	0.10	12500	100	(7),(12)
UM461	<21.0	...	...	13.6 $\pm$ 0.6	0.08	16100	200	(13),(14)
Tol1214-277	23.3 $\pm$ 2.8	...	...	...	0.03	19790	400	(15)
Tol65	<18.2	9.3 $\pm$ 0.4	...	...	0.08	17320	50	(7),(15)
Mrk1499	14.6 $\pm$ 1.9	15.1 $\pm$ 1.3	...	...	0.17	12600	3267	(7),(16)

REFERENCES. — (1) Bergvall & Oumlstlin (2002), (2) Guseva et al. (2000), (3) Izotov et al. (2006), (4) Hunt et al. (2004), (5) Houck et al. (2004b), (6) Kobulnicky & Skillman (1997), (7) Gil de Paz et al. (2003), (8) Ho et al. (1997), (9) Cannon et al. (2005), (10) Izotov et al. (1999a), (11) Izotov et al. (1997), (12) Izotov et al. (1994), (13) Moustakas & Kennicutt (2006), (14) Izotov & Thuan (1998), (15) Izotov et al. (2001), (16) Kong et al. (2002)

NOTE. — When no data are available in the literature, the electron temperature and densities are assumed to be 10 000 K (for NGC1140 and UGC4274) and 100 cm $^{-3}$  (for NGC1140 and NGC1569) respectively. When the Hu $\alpha$  line is detected, the H $\beta$  flux is preferentially derived from this line. The upper limits are listed for the non-detections. For the remaining sources, we derived the H $\beta$  flux either from the thermal component of the radio continuum, or from the extinction corrected H $\alpha$  flux inside the SH slit. For UM461, the H $\beta$  flux is for the whole galaxy from the integrated optical spectra.

faintness of our targets at  $\lambda < 9.7 \mu\text{m}$ , the determination of the continuum on the blue side of the  $9.7 \mu\text{m}$  feature is often poor and the uncertainties in estimating the mid-IR extinction from this are rather large (see discussion in Spoon et al. 2007). Thus for sources where optical spectra are available, we adopt the  $E_{B-V}$  values calculated from the hydrogen recombination lines in the literature. Only for SBS 0335-052E, which has a high quality mid-IR spectrum and evidence for an embedded SSC, the optical  $E_{B-V}$  is not a good estimate of its extinction, thus we use the extinction estimated from the depth of the silicate feature (Houck et al. 2004b). Throughout this paper, we adopt the Fluks et al. (1994) extinction law, though using the Draine (2003) law would produce very similar results. The  $E_{B-V}$  magnitudes are provided in Table 2.

### 3.4. Neon and sulfur abundances determination

We use the electron density and temperature given in Table 2, together with the fine structure lines detected in the *IRS* high-resolution spectra, to calculate the abundances of neon and sulfur. The equation used to determine the ionic abundance is described in Bernard Salas et al. (2001) and it is:

$$\frac{N_{\text{ion}}}{N_{\text{p}}} = \frac{I_{\text{ion}}}{I_{\text{H}\beta}} N_e \frac{\lambda_{\text{ul}}}{\lambda_{\text{H}\beta}} \frac{\alpha_{\text{H}\beta}}{A_{\text{ul}}} \left( \frac{N_{\text{u}}}{N_{\text{ion}}} \right)^{-1} \quad (1)$$

where  $I_{\text{ion}}/I_{\text{H}\beta}$  is the measured flux of the fine-structure line normalized to H $\beta$ ;  $N_{\text{p}}$  is the density of the ionized hydrogen;  $\lambda_{\text{ul}}$  and  $\lambda_{\text{H}\beta}$  are the wavelengths of the line and H $\beta$ ;  $\alpha_{\text{H}\beta}$  is the effective recombination coefficient for H $\beta$ ;  $A_{\text{ul}}$  is the Einstein spontaneous transition rate for the line and  $N_{\text{u}}/N_{\text{ion}}$  is the ratio of the population of the level from which the line originates to the total population of the ion. This ratio is determined by solving the statistical equilibrium equation for

a five level system and normalizing the total number of ions to be unity (Osterbrock 1989). The effective collisional strengths used to derive the population of levels were obtained from the appropriate reference of the IRON project (Hummer et al. 1993)<sup>7</sup>.

The most important ionization stages of neon and sulfur are available in the infrared. We detected [SIV]  $\lambda 10.51 \mu\text{m}$  and [NeIII]  $\lambda 15.56 \mu\text{m}$  in all of our BCDs while the [NeII]  $\lambda 12.81 \mu\text{m}$  line is detected in nine objects and [SIII]  $\lambda 18.71 \mu\text{m}$  in twelve sources (see Table 3). For sulfur, SII has its strongest emission lines in the optical. Vermeij et al. (2002) have shown that SII is typically less than 10% of SIII in the Magellanic cloud HII regions they studied. Because BCDs are typically high-excitation objects, we do not expect to have a significant contribution from SII. The optical studies reveal that the ionic abundance of SII is typically 10–20% of that of SIII (Izotov et al. 1994, 1997), thus we keep in mind that this might result in a  $\sim 10\%$  underestimate in our infrared derived sulfur abundance. This is addressed further in the following subsection where we discuss the properties of the individual objects. The presence of the [OIV]  $\lambda 25.89 \mu\text{m}$  line in most of our sources (except for VI Zw403, UM461, Tol65 and Mrk1499) indicates that some [NeIV] might be present, even though the [OIV] line is typically weak. For example, in Tol1214-277, where [OIV] is detected, the flux of [NeIV]  $\lambda 4725$  from optical spectra is less than 1% of that of [NeIII]  $\lambda 3868$  (Izotov et al. 2004), indicating that the contribution of [NeIV] is not significant. Tsamis & Péquignot (2005) also have shown in their photoionization modelling study of 30 Doradus that the contribution from NeIV to the total neon abundance is much less than 1%. As a result, rather than applying ionization correction factors

<sup>7</sup> <http://www.usm.uni-muenchen.de/people/ip/iron-project.html>

TABLE 3  
FINE-STRUCTURE LINE FLUXES AND IONIC ABUNDANCES

Object	Line Fluxes ( $\times 10^{-14} \text{ ergs cm}^{-2} \text{ s}^{-1}$ )				Ionic Abundances ( $\times 10^{-6}$ )			
	[SIV](10.51 $\mu\text{m}$ )	[NeII](12.81 $\mu\text{m}$ )	[NeIII](15.55 $\mu\text{m}$ )	[SIII](18.71 $\mu\text{m}$ )	N <sub>SIV</sub> /N <sub>p</sub>	N <sub>NeII</sub> /N <sub>p</sub>	N <sub>NeIII</sub> /N <sub>p</sub>	N <sub>SIII</sub> /N <sub>p</sub>
Haro11	43.95 $\pm$ 0.14	31.23 $\pm$ 0.23	98.14 $\pm$ 0.65	45.24 $\pm$ 0.25	0.353 $\pm$ 0.056	15.4 $\pm$ 2.4	23.2 $\pm$ 3.7	1.89 $\pm$ 0.30
NGC1140	12.14 $\pm$ 0.13	11.41 $\pm$ 0.20	37.79 $\pm$ 0.32	20.04 $\pm$ 0.11	0.375 $\pm$ 0.051	22.5 $\pm$ 3.0	35.5 $\pm$ 4.8	3.56 $\pm$ 0.48
SBS0335-052E	1.56 $\pm$ 0.03	<0.14	1.43 $\pm$ 0.02	0.43 $\pm$ 0.03	0.527 $\pm$ 0.011	<2.27	11.2 $\pm$ 1.6	0.535 $\pm$ 0.038
NGC1569	147.26 $\pm$ 0.55	15.70 $\pm$ 0.17	175.85 $\pm$ 0.59	72.70 $\pm$ 0.23	0.817 $\pm$ 0.040	5.28 $\pm$ 0.26	28.2 $\pm$ 1.4	2.12 $\pm$ 0.10
IIZw40	185.72 $\pm$ 1.73	6.24 $\pm$ 0.11	112.65 $\pm$ 0.83	45.80 $\pm$ 0.21	1.12 $\pm$ 0.03	2.23 $\pm$ 0.07	19.3 $\pm$ 0.6	1.37 $\pm$ 0.04
UGC4274	4.18 $\pm$ 0.12	8.87 $\pm$ 0.11	12.84 $\pm$ 0.12	12.63 $\pm$ 0.11	0.743 $\pm$ 0.068	102 $\pm$ 9	70.3 $\pm$ 6.1	13.2 $\pm$ 1.2
I Zw18	0.48 $\pm$ 0.03	0.09 $\pm$ 0.01	0.46 $\pm$ 0.02	0.23 $\pm$ 0.02	0.125 $\pm$ 0.015	1.41 $\pm$ 0.21	3.56 $\pm$ 0.38	0.276 $\pm$ 0.036
VIIZw403	0.99 $\pm$ 0.05	<0.142	0.88 $\pm$ 0.02	0.87 $\pm$ 0.02	0.311 $\pm$ 0.035	<2.79	8.41 $\pm$ 0.88	1.39 $\pm$ 0.14
Mrk1450	7.34 $\pm$ 0.04	1.34 $\pm$ 0.03	9.61 $\pm$ 0.04	4.37 $\pm$ 0.03	0.928 $\pm$ 0.223	10.70 $\pm$ 2.57	36.9 $\pm$ 8.9	2.98 $\pm$ 0.71
UM461	4.58 $\pm$ 0.04	0.16 $\pm$ 0.02	2.83 $\pm$ 0.03	0.812 $\pm$ 0.03	0.636 $\pm$ 0.029	1.38 $\pm$ 0.18	11.8 $\pm$ 0.5	0.563 $\pm$ 0.032
Tol1214-277	0.88 $\pm$ 0.02	<0.10	0.61 $\pm$ 0.02	<0.19	0.061 $\pm$ 0.007	<0.413	1.23 $\pm$ 0.15	<0.059
Tol65	0.69 $\pm$ 0.02	<0.14	0.90 $\pm$ 0.02	0.32 $\pm$ 0.02	0.129 $\pm$ 0.007	<1.62	5.07 $\pm$ 0.25	0.293 $\pm$ 0.022
Mrk1499	1.74 $\pm$ 0.02	1.88 $\pm$ 0.03	5.03 $\pm$ 0.03	2.91 $\pm$ 0.02	0.286 $\pm$ 0.037	16.5 $\pm$ 2.2	21.6 $\pm$ 2.8	2.28 $\pm$ 0.30

NOTE. — The observed line fluxes are measured from the IRS high resolution spectra of the sources. Background emission has not been subtracted, but this does not affect the flux of the fine-structure lines.

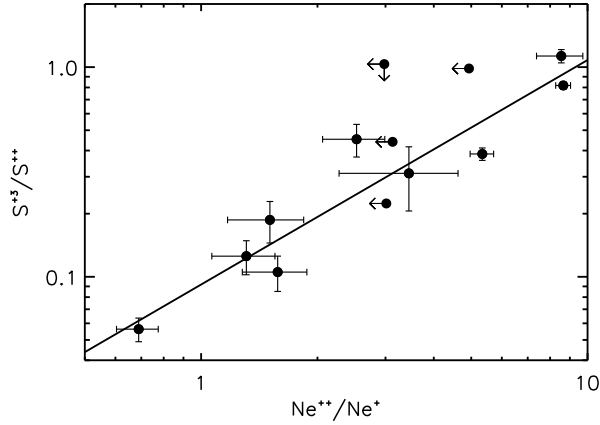


FIG. 1.— A plot of  $\text{Ne}^{++}/\text{Ne}^{+}$  vs  $\text{S}^{3+}/\text{S}^{++}$ , which traces the hardness of the radiation field. The solid line is a fit to the data.

(ICFs) which could introduce an unknown systematic uncertainty in our study, we sum the corresponding ionic abundances for the most important ionization stages to determine the total element abundance and the results are shown in Table 3.

Two successive stages of ionization of a given element (X) can be used to measure the state of the ionization of the ISM, which, on first order, depends on the ionization parameter, U, and the hardness of the ionizing radiation (Vilchez & Pagel 1988). For a given U, the ratio  $\text{X}^{i+1}/\text{X}^i$  is an indicator of the hardness of the stellar radiation field. Here we use the ionic pairs of  $\text{Ne}^{++}/\text{Ne}^{+}$  and  $\text{S}^{3+}/\text{S}^{++}$  as indicators of the hardness of the ionization field and plot them in Fig. 1. It is clear from the figure that these two ratios increase proportionally. This indicates that the hardening of the radiation field affects similarly the various elements in the full range of the ionizing continua.

The major uncertainty in our study of the elemental abundances originates from the  $\text{H}\beta$  fluxes used as references. For sources where the 12.37  $\mu\text{m}$   $\text{Hu}\alpha$  line is detected, we have no uncertainties from matching the slit apertures, and the extinction correction is very small.

For sources where we estimate the  $\text{H}\beta$  flux from the thermal radio continuum emission, we are free of extinction corrections, even though we still need to properly account for the radio emission which falls within the IRS slit. For BCDs with no  $\text{Hu}\alpha$  emission or radio data available in the literature, we estimate the  $\text{H}\beta$  flux using archival  $\text{H}\alpha$  images of the objects. This is clearly more challenging because in addition to the aperture corrections, the extinction correction is higher which could introduce a systematic uncertainty as large as 25%. In the following analysis, we indicate the sources with or without the detection of  $\text{Hu}\alpha$  line using different symbols on the plots (see Fig. 2, 3 and 4). The measurement uncertainties in the infrared lines are typically only a few percent, but could grow to  $\sim 10\%$  in the case of fainter sources. The uncertainties we list in Table 3 only account for measurement uncertainties.

### 3.5. Individual Objects

Some details on the individual objects and how we measured the necessary parameters are provided in the following paragraphs.

**Haro11:** The 12.37  $\mu\text{m}$   $\text{Hu}\alpha$  line is clearly detected in the SH spectrum. The source has multiple nuclei, designated as A, B and C (Bergvall & Oumlstlin 2002). The optical spectra from which the oxygen abundance was derived corresponds to the central region. Because all the lines we are using are from the SH spectrum, we are relatively free from extinction problems and there is no need for aperture correction. The contribution of SII may add  $\sim 10\%$  to the total sulfur abundance.

**NGC1140:** As with Haro11, the 12.37  $\mu\text{m}$   $\text{Hu}\alpha$  line is also clearly detected in the SH spectrum of NGC1140. No measurement was found in the literature for the electron temperature or density for this source, thus we assume 10000 K and  $100 \text{ cm}^{-3}$  respectively, which are typical for BCDs. However, because its oxygen abundance is more than half solar, the electron temperature could also be lower. If we use a  $T_e$  of 5000 K and re-derive the abundances, we find that the neon abundance would increase from  $5.8 \times 10^{-5}$  to  $8.5 \times 10^{-5}$  and the sulfur abundance from  $3.9 \times 10^{-6}$  to  $5.5 \times 10^{-6}$ . The contribution of SII may add  $\sim 10\%$  to the total sulfur abundance.

TABLE 4  
ELEMENTAL ABUNDANCES

Object	Ne/H ( $\times 10^{-6}$ )	S/H ( $\times 10^{-6}$ )	O/H ( $\times 10^{-5}$ )	Ne ( $Z_{\odot}$ )	S ( $Z_{\odot}$ )	O ( $Z_{\odot}$ )	ref (O/H)
Haro11	38.6 $\pm$ 4.4	2.24 $\pm$ 0.31	7.94	0.33 $\pm$ 0.04	0.16 $\pm$ 0.02	0.16	(1)
NGC1140	58.0 $\pm$ 5.7	3.94 $\pm$ 0.48	28.8	0.48 $\pm$ 0.05	0.28 $\pm$ 0.03	0.59	(2)
SBS0335-052E	[11.2, 13.5] <sup>a</sup>	1.06 $\pm$ 0.04	1.95 $\pm$ 0.09	[0.09, 0.11] <sup>a</sup>	0.08 $\pm$ 0.003	0.03 $\pm$ 0.001	(3)
NGC1569	33.5 $\pm$ 1.4	2.94 $\pm$ 0.11	15.8 $\pm$ 0.5	0.28 $\pm$ 0.01	0.21 $\pm$ 0.01	0.32 $\pm$ 0.01	(4)
II Zw40	21.5 $\pm$ 0.6	2.49 $\pm$ 0.05	12.2 $\pm$ 0.4	0.17 $\pm$ 0.005	0.18 $\pm$ 0.004	0.25 $\pm$ 0.01	(2)
UGC4274	172.3 $\pm$ 10.9	13.94 $\pm$ 1.20	33.3	1.4 $\pm$ 0.1	1.0 $\pm$ 0.1	0.68	(5)
IZw18	5.0 $\pm$ 0.4	0.40 $\pm$ 0.04	1.47 $\pm$ 0.09	0.04 $\pm$ 0.003	0.03 $\pm$ 0.003	0.03 $\pm$ 0.002	(6)
VI Zw403	[8.4, 11.2] <sup>a</sup>	1.70 $\pm$ 0.14	4.90 $\pm$ 0.11	[0.07, 0.09] <sup>a</sup>	0.12 $\pm$ 0.01	0.10 $\pm$ 0.002	(7)
Mrk1450	47.6 $\pm$ 9.2	3.98 $\pm$ 0.74	9.55 $\pm$ 0.11	0.40 $\pm$ 0.08	0.28 $\pm$ 0.06	0.19 $\pm$ 0.002	(8)
UM461	13.2 $\pm$ 0.5	1.20 $\pm$ 0.04	6.10 $\pm$ 0.40	0.11 $\pm$ 0.01	0.09 $\pm$ 0.003	0.12 $\pm$ 0.01	(9)
Tol1214-277	[1.2, 1.6] <sup>a</sup>	[0.06, 0.12] <sup>b</sup>	3.45 $\pm$ 0.10	[0.010, 0.013] <sup>a</sup>	[0.004, 0.008] <sup>b</sup>	0.07 $\pm$ 0.002	(10)
Tol65	[5.1, 6.7] <sup>a</sup>	0.42 $\pm$ 0.07	3.48 $\pm$ 0.10	[0.04, 0.06] <sup>a</sup>	0.03 $\pm$ 0.002	0.07 $\pm$ 0.02	(10)
Mrk1499	38.1 $\pm$ 3.6	2.57 $\pm$ 0.30	13.2	0.32 $\pm$ 0.03	0.18 $\pm$ 0.02	0.27	(11)

REFERENCES. — (1) Bergvall & Oumlstlin (2002), (2) Guseva et al. (2000), (3) Izotov et al. (2006), (4) Kobulnicky & Skillman (1997), (5) Ho et al. (1997), (6) Izotov et al. (1999a), (7) Izotov et al. (1997), (8) Izotov et al. (1994), (9) Izotov & Thuan (1998), (10) Izotov et al. (2001), (11) Kong et al. (2002)

NOTE. — We adopt the following values for the solar abundances:  $(\text{Ne}/\text{H})_{\odot}=1.2 \times 10^{-4}$ ,  $(\text{S}/\text{H})_{\odot}=1.4 \times 10^{-5}$  and  $(\text{O}/\text{H})_{\odot}=4.6 \times 10^{-4}$  (See section 4.1).

<sup>a</sup> We provide a range for the neon abundance by taking as the lower value the ionic abundance of NeIII, while to obtain the upper value we add the upper limit for NeII.

<sup>b</sup> We provide a range for the sulfur by taking as the lower value the ionic abundance of SIV, while to obtain the upper value we add the upper limit of SIII.

**SBS0335-052E:** We do not detect the 12.37  $\mu\text{m}$   $\text{H}\alpha$  line in the SH spectrum. We use the thermal component of the 5 GHz radio continuum from Hunt et al. (2004) to convert to the  $\text{H}\beta$  flux, and thus no extinction correction is needed. [NeII] is not detected and we provide the upper limit in Table 3. The ionic abundance of SII is  $\sim 25\%$  of the SIII determined from the optical study of Izotov et al. (2006) and may add 12% to the total sulfur abundance. We also find higher neon and sulfur abundances compared with the oxygen and possible implications are discussed in Houck et al. (2004b).

**NGC1569:** The 12.37  $\mu\text{m}$   $\text{H}\alpha$  line is clearly detected in the SH spectrum, thus providing a direct estimate of the  $\text{H}\beta$  flux inside the SH slit. This galaxy is extended in the mid-IR (see Fig. 4 in Wu et al. 2006) and optical spectra have been taken for several of the bright knots by Kobulnicky & Skillman (1997) in order to study the chemical gradient and inhomogeneities of the source. These authors found very little variation in the metallicity. Our infrared-derived abundances are in rough agreement with the optical results. The ionic abundance of SII is  $\sim 13\%$  that of the SIII estimated from the optical study (Kobulnicky & Skillman 1997) and may add 9% to the total sulfur abundance.

**II Zw40:** We use the 12.37  $\mu\text{m}$   $\text{H}\alpha$  line to convert to  $\text{H}\beta$  flux. The derived neon and sulfur abundances agree with each other but appear to be lower than oxygen with respect to the solar values. If we estimate the  $\text{H}\beta$  flux from the  $\text{H}\alpha$  image of Gil de Paz et al. (2003), we find a value  $\sim 22\%$  lower than the first, which would increase the neon and sulfur abundances by 22% accordingly. This suggests, that when using the  $\text{H}\beta$  flux derived from  $\text{H}\alpha$  image, the systematic error in our measurement is probably no better than 25%. The ionic abundance of SII is  $\sim 13\%$  that of SIII from the optical study of Guseva et al. (2000) and may add 7% to the total sulfur abundance.

**UGC4274:** We use an  $\text{H}\beta$  flux derived from the  $\text{H}\alpha$  image of Gil de Paz et al. (2003). Similarly to NGC1569,

the galaxy is extended and the peak of the infrared centroid is displaced from the optical peak position. The derived neon and sulfur abundances are both super solar. The oxygen abundance is not directly available from the literature, thus we use the [NII]/ $\text{H}\alpha$  method (Ho et al. 1997; Denicoló et al. 2002) to derive O/H, which bears a large uncertainty. The contribution of SII may add  $\sim 10\%$  to the total sulfur abundance.

**IZw18:** The  $\text{H}\beta$  flux is derived from the thermal component of the radio continuum inside the SH slit. The ionic abundance of SII is  $\sim 21\%$  that of SIII from the optical study of Izotov et al. (1999a) and may add 15% to the total sulfur abundance. A more detailed discussion on this object can be found in Wu et al. (2007).

**VI Zw403:** The  $\text{H}\beta$  flux is derived by using the  $\text{H}\alpha$  image from Gil de Paz et al. (2003). The optical and infrared centroids do not overlap. The SH spectrum for this source is noisy and [NeII]  $\lambda 12.81 \mu\text{m}$  is not detected, thus we have only a lower limit on the neon abundance. The upper limit of the [NeII] line indicates that it could add less than 25% to the total elemental abundance of neon which is presented in Table 4. The ionic abundance of SII is  $\sim 24\%$  that of SIII from the optical work of Izotov et al. (1997) and may add 20% to the total sulfur abundance.

**Mrk1450:** As with VI Zw403, we use the hydrogen flux as given by the  $\text{H}\alpha$  flux included in the SH slit. Neon and sulfur abundances appear to be higher than the oxygen abundance with respect to the solar values. The ionic abundance of SII is  $\sim 18\%$  that of SIII from the optical study of Izotov et al. (1994) and may add 12% to the total sulfur abundance.

**UM461:** The  $\text{H}\beta$  flux is estimated from the integrated spectra of Moustakas & Kennicutt (2006), and the source is small enough to be fully included by the SH slit. The derived neon and sulfur abundances are in good agreement with oxygen metallicity from the optical. The ionic abundance of SII is  $\sim 17\%$  that of SIII from the

optical (Izotov & Thuan 1998) and may add 8% to the total sulfur abundance.

**Tol1214-277:** The  $12.37\ \mu\text{m}$   $\text{H}\alpha$  line is marginally detected in the SH spectrum, and we use this line to derive the  $\text{H}\beta$  flux. The spectrum is very noisy and no  $[\text{NeII}]\ \lambda 12.81\ \mu\text{m}$  or  $[\text{SIII}]\ \lambda 18.71\ \mu\text{m}$  lines are visible. We use the ionic abundances of  $[\text{NeIII}]$  and  $[\text{SIV}]$  as the lower limits of the neon and sulfur abundances. The upper limit of  $[\text{NeII}]$  amounts to 33% of the ionic abundance of  $[\text{NeIII}]$  while the upper limit of  $[\text{SIII}]$  is nearly as much as the abundance of  $[\text{SIV}]$ . We give the range of their elemental abundances in Table 4. The ionic abundance of SII is  $\sim 18\%$  that of SIII from the optical study of Izotov et al. (2001) and may add  $\sim 9\%$  to the total sulfur abundance.

**Tol65:** We use the  $\text{H}\alpha$  image (Gil de Paz et al. 2003) to calculate the  $\text{H}\beta$  flux.  $[\text{NeII}]\ \lambda 12.81\ \mu\text{m}$  is not detected in the SH spectrum, thus our derived neon abundance is a lower limit. The upper limit of NeII is  $\sim 32\%$  of the ionic abundance of NeIII, and the range of neon abundance is provided in Table 4. The metallicity of sulfur relative to solar is lower than oxygen. The ionic abundance of SII is  $\sim 26\%$  that of SIII from the optical (Izotov et al. 2001) and may add 19% to the total sulfur abundance.

**Mrk1499:** The  $12.37\ \mu\text{m}$   $\text{H}\alpha$  line is detected in the SH spectrum. There was a bad pixel at the peak of this line and we interpolated its value using adjacent pixel values. The infrared centroid appears to be slightly shifted from the optical one. The  $\text{H}\beta$  flux inside the SH slit derived from the  $\text{H}\alpha$  image is very similar to that derived from the  $\text{H}\alpha$  line (within  $\sim 10\%$ ). The contribution of SII may add  $\sim 10\%$  to the total sulfur abundance.

#### 4. DISCUSSION

In this section, we compare the abundances derived from the IR spectra with the results from the optical studies.

##### 4.1. Solar abundances

The solar photospheric abundances have changed drastically over the past few years (see discussion in Pottasch & Bernard-Salas 2006). In some cases, the solar abundance estimates for the same element from different authors could differ by a factor of two. In this paper, when we quote the elemental abundance in solar units (e.g. Table 4), we adopt the following values:  $(\text{Ne}/\text{H})_{\odot} = 1.2 \times 10^{-4}$  from Feldman & Widing (2003),  $(\text{S}/\text{H})_{\odot} = 1.4 \times 10^{-5}$  from Asplund et al. (2005), and  $(\text{O}/\text{H})_{\odot} = 4.9 \times 10^{-4}$  from Allende Prieto et al. (2001). We should note though that Asplund et al. (2005) have also reported that  $(\text{Ne}/\text{H})_{\odot} = 6.9 \times 10^{-5}$  and Grevesse & Sauval (1998) have given  $(\text{S}/\text{H})_{\odot} = 2.1 \times 10^{-5}$ , while Anders & Grevesse (1989) have reported that  $(\text{O}/\text{H})_{\odot} = 8.5 \times 10^{-4}$ . These values represent the extremes for the solar neon, sulfur and oxygen abundance determinations. Pottasch & Bernard-Salas (2006) have shown that the higher neon solar value is favored in their sample of planetary nebulae (PNe). In the present paper we indicate the range of solar abundances in our plots and we also discuss the impact of different solar values on our results.

##### 4.2. Neon and sulfur abundances

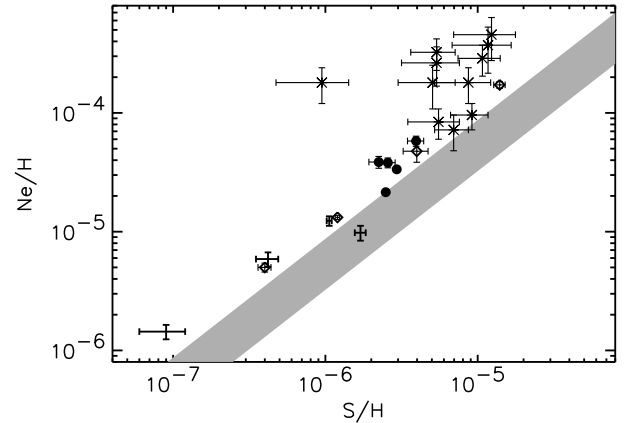


FIG. 2.— A plot of the  $\text{Ne}/\text{H}$  vs  $\text{S}/\text{H}$  abundance. Our BCDs are indicated by the plot of the filled circles if  $\text{H}\alpha$  is detected and by diamonds if it is not detected. The sources that are shown by only the error bars are those that have non-detection of  $[\text{NeII}]$  or  $[\text{SIII}]$  (See note of Table 4). The starburst galaxies from Verma et al. (2003) are marked with the stars. We use the grey band to indicate the locus on the plot where the ratio of  $\text{Ne}/\text{S}$  would be consistent with the different solar values for neon and sulfur abundances.

As discussed in Thuan et al. (1995), it is assumed — and has been shown in the optical — that the  $\alpha$ -element-to-oxygen abundance ratios do not vary with oxygen abundance. This is due to the fact that those elements are produced by the same massive stars ( $M > 10 M_{\odot}$ ) responsible for oxygen production. We test this assumption in the infrared by studying the abundances of neon and sulfur as derived from our IRS data.

In Fig. 2, we plot the abundances of neon and sulfur as derived from our high-resolution data. Verma et al. (2003) have found a positive correlation between the neon and argon abundances for their sample of starburst galaxies while their data show no correlation between the sulfur and neon and/or argon abundances (indicated as stars on Fig. 2). However, our sources show that the neon and sulfur abundances scale with each other. In the same figure, we also plot the proportionality line of the ratio for  $(\text{Ne}/\text{S})_{\odot}$ . The maximum and minimum values of the solar neon and sulfur abundances are indicated by the width of the grey band, and we find that most of our BCDs have ratios above those values.

In Fig. 3, we examine the ratio of  $\text{Ne}/\text{S}$  as a function of  $\text{Ne}/\text{H}$  derived from the IRS data. We see no correlation between the ratio of  $\text{Ne}/\text{S}$  with respect to  $\text{Ne}/\text{H}$ , in agreement with the results of Thuan et al. (1995). The average  $\text{Ne}/\text{S}$  ratio we found for these BCDs is  $\sim 11.4$ . This is similar with the  $\text{Ne}/\text{S}$  ratio of 14.3 in the Orion Nebula (Simpson et al. 2004). The  $\text{Ne}/\text{S}$  ratios found in the HII regions of M83 are higher ( $\sim 24$ – $42$ ) and decrease with increasing deprojected galactocentric radii (Rubin et al. 2007). These authors have also found that the  $\text{Ne}/\text{S}$  ratios in M33 are  $\sim 12$ – $21$  (Rubin et al. 2006). We notice that all the BCDs, as well as the HII regions in M33, M83 and the Orion Nebula, have larger  $\text{Ne}/\text{S}$  ratios than those found in the solar neighborhood, while their  $\text{Ne}/\text{S}$  ratios from optical measurements are more consistent with the solar ratios. The higher  $\text{Ne}/\text{S}$  ratios from infrared studies have already been found in other type of objects, including PNe, starburst galaxies, and other HII regions

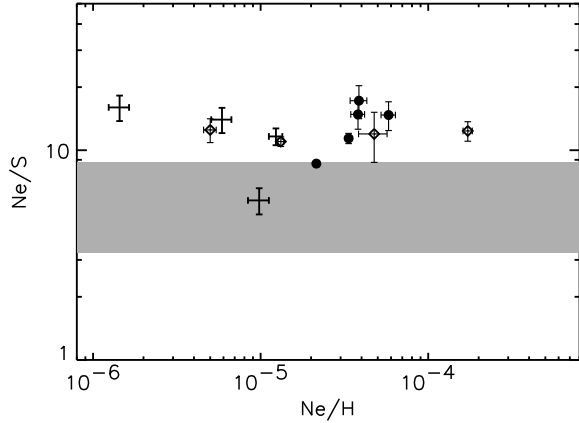


FIG. 3.— The abundance ratio of Ne/S as a function of Ne/H. The symbols are the same as in Fig. 1. The grey area indicates the range for the values of the Ne/S ratio encountered in the solar neighborhood.

(Marigo et al. 2003; Verma et al. 2003; Henry et al. 2004; Pottasch & Bernard-Salas 2006). Some of these works point out that the solar sulfur abundance could have been underestimated and they also appear to favor the higher values for the solar neon abundance. It could also be due to a differential depletion of sulfur onto dust grains compared to neon as suggested by several studies (Simpson & Rubin 1990; Verma et al. 2003; Pottasch & Bernard-Salas 2006; Bernard Salas et al. 2007).

#### 4.3. Comparison with optically derived abundances

As has been discussed earlier in this paper, one of the major advantages of using IR lines for estimating abundances is that one can probe emission from dust enshrouded regions without the uncertainties introduced from extinction corrections. In this subsection, we compare the newly derived neon and sulfur abundances of our BCD sample using the infrared data, with the abundances of the same elements as well as those for oxygen estimated from optical studies available in the literature.

In order to determine elemental abundances, the optical studies usually adopt a two-zone photoionized HII region model: a high-ionization zone with temperature  $T_e(\text{OIII})$  and a low-ionization zone with temperature  $T_e(\text{OII})$ . Because the infrared lines are much less sensitive to variations in  $T_e$  (which affect the calculation on the population of the various atomic levels), in the subsequent calculations, we assume a constant electron temperature for our analysis.

In Fig. 4 we compare the infrared derived neon and sulfur abundances of the BCD sample with their optical metallicities, using the oxygen abundances from the literature (see also Table 4). The infrared neon abundances with respect to solar are slightly higher than the oxygen (see Fig. 4a), but overall, there is a good agreement between the infrared measurements and the optical results. This indicates that there is little dust enshrouded gas, or that these regions have similar metallicities, or that they do not contribute much to the total integrated emission of the galaxies. In SBS0335-052E, as well as Mrk1450, UGC4274 and Haro11, the infrared derived metallicity of neon is more than twice that of oxygen compared to the

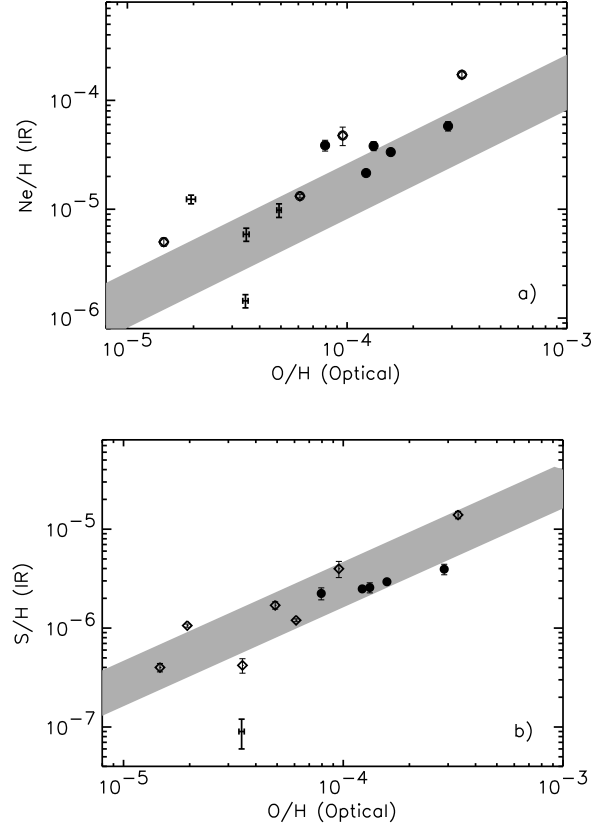


FIG. 4.— a) The Ne/H vs O/H abundances. The symbols are the same as in Fig. 1. The grey band represents the locus on the plot where sources of different metallicities would have a Ne/O intrinsic ratio similar to the values found in the solar neighborhood. b) Same as a), but for S/H vs O/H abundances.

solar values. This could be due to the different regions we are probing using the infrared, which could be obscured in the optical. SBS0335-052E is known to have an embedded super star cluster that is invisible in the optical (see Houck et al. 2004b). Both Haro11 and UGC4274 are somewhat extended, and detailed spectroscopy over the whole galaxy would be needed to directly compare the infrared results with the optical ones. For Mrk1450, which is a point source for Spitzer/IRS, the abundance we derived using the infrared data is higher than the optical value and it is likely due to the fact that the optical estimates are more susceptible to the uncertainties in the electron temperature. If we lower  $T_e$  from 12 500 K to 10 000 K, the oxygen abundance calculated from the optical data would double, while the neon abundance measured from the infrared would only increase by 5%. In Fig. 4b we show that the infrared derived sulfur abundances agree well with the oxygen abundance relative to solar.

For nine out of the thirteen objects we studied, optically derived neon and sulfur abundances are also available in the literature. The optical data have matched apertures, in most cases an accurate  $T_e$  measurement, a direct measure of the  $H\beta$  flux, and reddening derived from the same data. Our infrared results are less sensitive to the electron temperature, but affected by the uncertainty in the  $H\beta$  flux if the  $H\alpha$  line is not de-



TABLE 5  
PAH MEASUREMENTS OF THE SAMPLE

Object Name	PAH EW ( $\mu\text{m}$ )				Integrated Flux ( $\times 10^{-14} \text{ ergs cm}^{-2} \text{ s}^{-1}$ )			
	6.2 $\mu\text{m}$	7.7 $\mu\text{m}$	8.6 $\mu\text{m}$	11.2 $\mu\text{m}$	6.2 $\mu\text{m}$	7.7 $\mu\text{m}$	8.6 $\mu\text{m}$	11.2 $\mu\text{m}$
Haro11	0.120 $\pm$ 0.003	0.227 $\pm$ 0.005	0.042 $\pm$ 0.003	0.099 $\pm$ 0.002	78.3 $\pm$ 1.8	180 $\pm$ 4	25.4 $\pm$ 1.6	67.2 $\pm$ 1.3
NGC1140	0.479 $\pm$ 0.033	0.568 $\pm$ 0.024	0.091 $\pm$ 0.006	0.525 $\pm$ 0.032	42.1 $\pm$ 1.4	78.3 $\pm$ 1.8	11.1 $\pm$ 0.7	50.2 $\pm$ 2.5
SBS0335-052E	<0.035	...	...	<0.015	<1.7	...	...	<1.0
NGC1569	0.232 $\pm$ 0.013	0.380 $\pm$ 0.019	0.007 $\pm$ 0.005	0.129 $\pm$ 0.008	50.4 $\pm$ 2.4	118 $\pm$ 6	2.7 $\pm$ 1.6	68.1 $\pm$ 4.3
II Zw40	0.044 $\pm$ 0.007	0.044 $\pm$ 0.006	0.006 $\pm$ 0.005	0.033 $\pm$ 0.006	13.2 $\pm$ 2.1	19.0 $\pm$ 2.8	2.8 $\pm$ 1.2	21.1 $\pm$ 3.7
UGC4274	0.423 $\pm$ 0.032	0.497 $\pm$ 0.049	0.105 $\pm$ 0.012	0.495 $\pm$ 0.021	23.2 $\pm$ 1.2	43.3 $\pm$ 2.3	7.7 $\pm$ 0.9	29.1 $\pm$ 0.9
IZw18	<0.233	...	...	<0.116	<0.4	...	...	<0.1
Mrk1450	0.207 $\pm$ 0.045	0.337 $\pm$ 0.143	0.084 $\pm$ 0.020	0.112 $\pm$ 0.017	1.8 $\pm$ 0.4	2.8 $\pm$ 0.9	0.7 $\pm$ 0.2	1.6 $\pm$ 0.2
UM461	<0.663	...	...	<0.134	<1.5	...	...	<1.6
Mrk1499	0.408 $\pm$ 0.040	0.526 $\pm$ 0.016	0.156 $\pm$ 0.011	0.721 $\pm$ 0.035	5.5 $\pm$ 0.3	10.9 $\pm$ 0.3	2.3 $\pm$ 0.2	7.3 $\pm$ 0.2

NOTE. — Contrary to Wu et al. (2006), the wavelengths which we have chosen to determine the underlying continuum are fixed in the above measurements, which explains the minor discrepancies between these two studies. The symbol “...” indicates that no PAH EW measurement was possible and it is mostly due to the low SNR of the corresponding spectrum. In this case, the determination of the continuum is highly uncertain and could significantly affect the value of the PAH EW. For SBS0335-052E, the SNR is high enough, but no PAH features can be identified in its mid-IR spectrum. We do not derive upper limits for the PAH EWs at 7.7  $\mu\text{m}$  and 8.6  $\mu\text{m}$ , because no reliable templates for those features are available.

tected and the uncertainty could be as large as 25%. In Fig. 5a, we plot the optically derived Ne/H against the infrared Ne/H. The solid line is the 1:1 proportion line for the infrared and optical derived abundances and we find that most of the sources are located above this line. A possible explanation for the higher infrared derived neon abundances could be the presence of dust enshrouded regions which might have higher heavy element abundances. This could explain the higher infrared metallicity found in SBS0335-052E, but if this were true for the whole sample, it should also apply to the sulfur abundances. However, when we plot the S/H (Optical) against the S/H (IR) in Fig. 5b, we find that the sources are located on both sides of the 1:1 proportion line. Alternatively, this could be due to the difference in the determination of element abundance using the infrared and optical methods. Because only NeIII is detected in the optical regime, the total elemental abundance of neon from the optical study is heavily dependent on the adopted ICF. In the infrared the [NeII] line is detected in most of our sources and we do not use any ICF for our study. Thus the higher neon abundances derived from the infrared data compared to the optical results could also be due to the large uncertainty in the ICF used in the optical studies. Another possibility is that the temperature of the NeIII ion is lower than that of the OIII ion as found in some PNe (Bernard Salas et al. 2002). Because the optical studies are based on  $T_e(\text{OIII})$  when calculating the ionic abundance of NeIII, that could also result in an underestimate of its abundance.

Finally, we explore the variation in the ratio of Ne/S as derived from the infrared and the optical data, and plot them as a function of O/H in Fig. 6. Interestingly, we find that with the exception of VI Zw403, in all BCDs, the infrared derived Ne/S ratios are higher than the corresponding optical values. Izotov & Thuan (1999b) indicate an average Ne/S ratio of 6.9 for the 54 super giant HII regions they study in 50 BCDs using optical spectroscopy. The average of the optically derived Ne/S ratio for the nine sources in our sample is  $6.5 \pm 1.8$  while the corresponding ratio from the infrared data is  $11.4 \pm 2.9$ , statistically higher than the optical results. As we mentioned earlier, no SII abundances could be de-

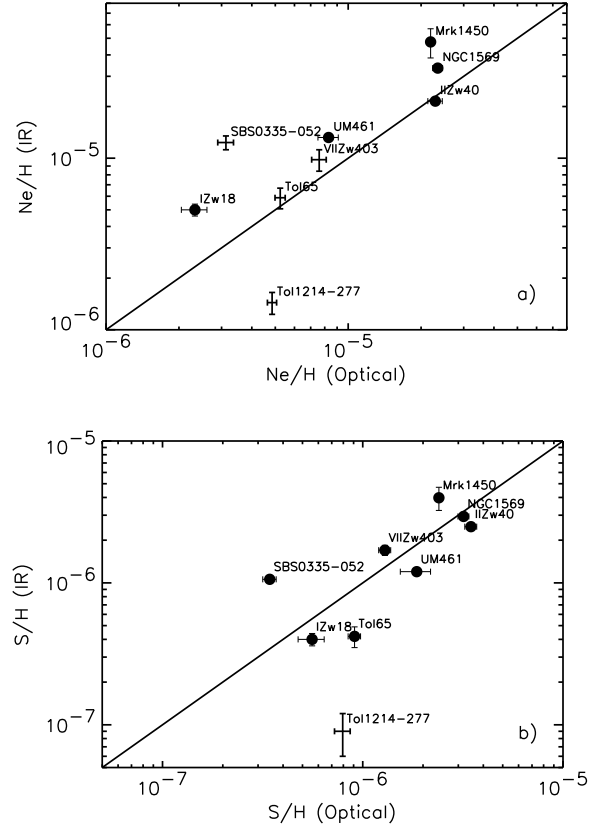


FIG. 5.— a) The infrared derived Ne/H as a function of the optical Ne/H abundances. The sources shown with only the error bars are those where [NeII] or [SIII] is not detected. The solid line represents the 1:1 line for the optical and IR derived abundances. b) Same as a), but for S/H (Optical) vs S/H (IR) abundances.

termined with the Spitzer/IRS data. However, in high-excitation objects such as BCDs, SII does not contribute much ( $\sim 10\%$ ) to the total elemental abundance, thus it could not account for the factor of two difference in the ratio of Ne/S. Furthermore, such a discrepancy is not a result of metallicity because we see no correlation in the

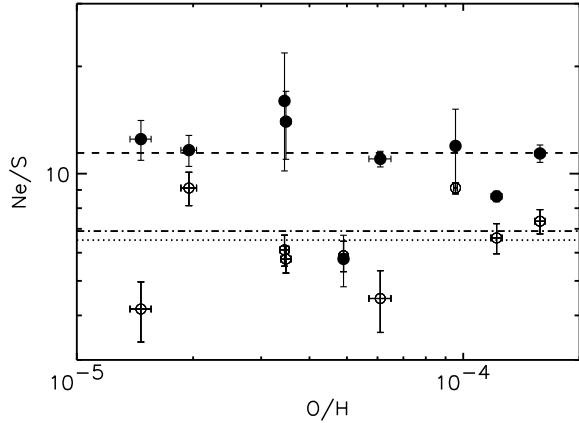


FIG. 6.— The abundance ratio of Ne/S as a function of O/H. The infrared derived Ne/S ratios are indicated by the filled circles while the optical derived Ne/S ratios are shown by the open circles. The dashed line is the average Ne/S ratio from the infrared derived elemental abundances while the dotted line is average Ne/S ratio from the optical derived elemental abundances. The dash-dotted line represents the average Ne/S ratio from Izotov & Thuan (1999b).

dispersion between the infrared and optically derived ratios of Ne/S with respect to O/H. If we divide the sources into a high-excitation group with sources that have a detectable [OIV] $\lambda$ 25.89  $\mu$ m line and a low-excitation group with sources without any detection of [OIV], we still see no clear trend. Thus the ionization field cannot explain the difference in the Ne/S ratios either. Moreover, no correlation is found between the Ne/S ratio and the extinction to the source. Even though the largest uncertainty in the infrared derived abundances comes from the uncertainty in the H $\beta$  flux in cases where no H $\alpha$  is detected, when calculating the ratio of Ne/S, the H $\beta$  flux cancels out, thus our infrared determined values for Ne/S should be fairly reliable. One possibility for the observed discrepancy could be that the difference in the infrared and optical results is again due to the ICF adopted in the optical studies.

##### 5. METALLICITIES AND PAHS

The observed suppression of PAH emission in low metallicity environment is still an open topic (Madden 2000; Madden et al. 2006; Engelbracht et al. 2005; Wu et al. 2006; O’Halloran et al. 2006). One explanation on the absence of PAHs is that there is not enough carbon to form into PAH molecules in such metal-poor environments while an alternative possibility could be that the strong ionization field in low metallicity environments may destroy the fragile PAH rings.

Previous studies relating the PAHs and metallicity were all based on the oxygen abundance measured from the optical, which could be associated with regions that are different from the ones where PAH emission originates. Because we have obtained the infrared measured neon and sulfur abundances, it is particularly interesting to compare the PAH strength with our metallicity

estimates. Several BCDs in our sample do show PAH emission features and an analysis of the PAH properties of our sample based on IRS low resolution spectra was presented in Wu et al. (2006). We have obtained deeper spectra for some of the sources, so for consistency, we have re-measured all features in our sample and the results are given in Table 5. None of the sources with metallicity lower than  $\sim 0.12 Z_{\odot}$  show any detectable PAHs. For the sources where PAHs were detected, we calculate the equivalent widths (EWs) of the 6.2, 7.7, 8.6 and 11.2  $\mu$ m features and find that the correlation between the PAH EWs and the metallicity is weak. This is not unexpected because as discussed in Wu et al. (2006), the strength of PAHs in low-metallicity environments is a combination of creation and destruction effects. As a result the dependency of PAH strength on the metallicity alone could have a substantial scatter.

##### 6. CONCLUSIONS

We have studied the neon and sulfur abundances of thirteen BCDs using Spitzer/IRS high-resolution spectroscopy. Our analysis was based on the fine-structure lines and the hydrogen recombination line detected in the SH spectra of the IRS, combined with the radio continuum, H $\alpha$  images and integrated optical spectral data in some cases. We find a positive correlation between the neon and sulfur abundances, though sulfur appears to be more under-abundant than neon (with respect to solar). The ratio of Ne/S for our sources is on average  $11.4 \pm 2.9$ , which is consistent with what has been found in other HII regions using infrared data. However, this average ratio appears to be higher than the corresponding optical value of  $6.5 \pm 1.8$  (in BCDs), which could be due to the adopted ICFs in the optical studies. When comparing the newly derived neon and sulfur abundances with the oxygen abundances measured from the optical lines, we find a good overall agreement. This indicates that there are few completely dust enshrouded HII regions in our BCDs, or if such HII regions are present, they have similar metallicities to the ones probed in the optical. Finally, the infrared derived neon and sulfur abundances also correlate, with some scatter, with the corresponding elemental abundances derived from the optical data.

We thank Robert Kennicutt whose detailed comments help to improve this manuscript. We also thank Shannon Gutenkunst and Henrik Spoon for helpful discussions as well as an anonymous referee whose insightful suggestions helped to improve this manuscript. This work is based in part on observations made with the Spitzer Space Telescope, which is operated by the Jet Propulsion Laboratory, California Institute of Technology, under NASA contract 1407. Support for this work was provided by NASA through Contract Number 1257184 issued by JPL/Caltech.

##### REFERENCES

- Anders, E., & Grevesse, N. 1989, *Geochim. Cosmochim. Acta*, 53, 197
- Allende Prieto, C., Lambert, D. L., & Asplund, M. 2001, *ApJ*, 556, L63

- Aloisi, A. et al. 2007, astro-ph/0702216, Proceedings of the IAU Symp. 241 “Stellar Populations as Building Blocks of Galaxies”
- Aloisi, A., Savaglio, S., Heckman, T.M., Hoopes, C. G., Leitherer, C., & Sembach, K. R. 2003, ApJ, 595, 760
- Asplund, M., Grevesse, N., & Sauval, A. J. 2005, Cosmic Abundances as Records of Stellar Evolution and Nucleosynthesis, 336, 25
- Bergvall, N., & Oumlstlin, G. 2002, A&A, 390, 891
- Becker, R. H., White, R. L., & Helfand, D. J. 1995, ApJ, 450, 559
- Bernard Salas, J., et al. 2007, ApJ, in press, astro-ph/0709.3292
- Bernard Salas, J., Pottasch, S. R., Feibelman, W. A., & Wesselius, P. R. 2002, A&A, 387, 301
- Bernard Salas, J., Pottasch, S. R., Beintema, D. A., & Wesselius, P. R. 2001, A&A, 367, 949
- Cannon, J. M., Walter, F., Skillman, E. D., & van Zee, L. 2005, ApJ, 621, L21
- Cohen, M., Megeath, S. T., Hammersley, P. L., Martín-Luis, F., & Stauffer, J. 2003, AJ, 125, 2645
- Denicoló, G., Terlevich, R., & Terlevich, E. 2002, MNRAS, 330, 69
- Draine, B. T. 2003, ARA&A, 41, 241
- Engelbracht, C. W., Gordon, K. D., Rieke, G. H., Werner, M. W., Dale, D. A., & Latter, W. B. 2005, ApJ, 628, L29
- Feldman, U., & Widing, K. G. 2003, Space Science Reviews, 107, 665
- Fluks, M. A., Plez, B., The, P. S., de Winter, D., Westerlund, B. E., & Steenman, H. C. 1994, A&AS, 105, 311
- Gil de Paz, A., Madore, B. F., & Pevunova, O. 2003, ApJS, 147, 29
- Grevesse, N., & Sauval, A. J. 1998, Space Science Reviews, 85, 161
- Guseva, N. G., Izotov, Y. I., & Thuan, T. X. 2000, ApJ, 531, 776
- Hao, L., et al. 2007, in preparation
- Henry, R. B. C., Kwitter, K. B., & Balick, B. 2004, AJ, 127, 2284
- Higdon, S. J. U., et al. 2004, PASP, 116, 975
- Ho, L. C., Filippenko, A. V., & Sargent, W. L. W. 1997, ApJS, 112, 315
- Hogg, D. W., Tremonti, C. A., Blanton, M. R., Finkbeiner, D. P., Padmanabhan, N., Quintero, A. D., Schlegel, D. J., & Wherry, N. 2005, ApJ, 624, 162
- Houck, J. R., et al. 2004a, ApJS, 154, 18
- Houck, J. R., et al. 2004b, ApJS, 154, 211
- Houck, J. R., Shure, M. A., Gull, G. E., & Herter, T. 1984, ApJ, 287, L11
- Hummer, D. G., Berrington, K. A., Eissner, W., Pradhan, A. K., Saraph, H. E., & Tully, J. A. 1993, A&A, 279, 298
- Hummer, D. G., & Storey, P. J. 1987, MNRAS, 224, 801
- Hunt, L. K., Thuan, T. X., Sauvage, M., & Izotov, Y. I. 2006, ApJ, 653, 222
- Hunt, L., Bianchi, S., & Maiolino, R. 2005a, A&A, 434, 849
- Hunt, L. K., Dyer, K. K., Thuan, T. X., & Ulvestad, J. S. 2004, ApJ, 606, 853
- Hunter, D. A., & Hoffman, L. 1999, AJ, 117, 2789
- Izotov, Y. I., Thuan, T. X., & Lipovetsky, V. A. 1994, ApJ, 435, 647
- Izotov, Y. I., Thuan, T. X., & Lipovetsky, V. A. 1997, ApJS, 108, 1
- Izotov, Y. I., & Thuan, T. X. 1998, ApJ, 500, 188
- Izotov, Y. I., Chaffee, F. H., Foltz, C. B., Green, R. F., Guseva, N. G., & Thuan, T. X. 1999, ApJ, 527, 757
- Izotov, Y. I., & Thuan, T. X. 1999, ApJ, 511, 639
- Izotov, Y. I., Chaffee, F. H., & Green, R. F. 2001, ApJ, 562, 727
- Izotov, Y. I., Papaderos, P., Guseva, N. G., Fricke, K. J., & Thuan, T. X. 2004, A&A, 421, 539
- Izotov, Y. I., Thuan, T. X., & Guseva, N. G. 2005, ApJ, 632, 210
- Izotov, Y. I., Schaerer, D., Blecha, A., Royer, F., Guseva, N. G., & North, P. 2006, A&A, 459, 71
- Kirshner, R. P., Oemler, A., Jr., Schechter, P. L., & Shectman, S. A. 1981, ApJ, 248, L57
- Kniazev, A. Y., Grebel, E. K., Hao, L., Strauss, M. A., Brinkmann, J., & Fukugita, M. 2003, ApJ, 593, L73
- Kobulnicky, H. A., & Skillman, E. D. 1997, ApJ, 489, 636
- Kong, X., Cheng, F. Z., Weiss, A., & Charlot, S. 2002, A&A, 396, 503
- Kunth, D., & Östlin, G. 2000, A&A Rev., 10, 1
- Kunth, D., & Sargent, W. L. W. 1986, ApJ, 300, 496
- Lebouteiller, V., Kunth, D., Lequeux, J., Lecavelier des Etangs, A., Désert, J.-M., Hébrard, G., & Vidal-Madjar, A. 2004, A&A, 415, 55
- Loose, H.-H., & Thuan, T. X. 1985, Star-Forming Dwarf Galaxies and Related Objects, 73
- Madden, S. C., Galliano, F., Jones, A. P., & Sauvage, M. 2006, A&A, 446, 877
- Madden, S. C. 2000, New Astronomy Review, 44, 249
- Marigo, P., Bernard-Salas, J., Pottasch, S. R., Tielens, A. G. G. M., & Wesselius, P. R. 2003, A&A, 409, 619
- Martín-Hernández, N. L., et al. 2002, A&A, 381, 606
- Martín-Hernández, N. L., Schaerer, D., Peeters, E., Tielens, A. G. G. M., & Sauvage, M. 2006, A&A, 455, 853
- Melbourne, J., & Salzer, J. J. 2002, AJ, 123, 2302
- Moustakas, J., & Kennicutt, R. C., Jr. 2006, ApJS, 164, 81
- O’Halloran, B., Satyapal, S., & Dudik, R. P. 2006, ApJ, 641, 795
- Osterbrock, D. E. 1989, Astrophysics of gaseous nebulae and active galactic nuclei. Research supported by the University of California, John Simon Guggenheim Memorial Foundation, University of Minnesota, et al. Mill Valley, CA, University Science Books, 1989, 422p
- Peimbert, M., & Torres-Peimbert, S. 1992, A&A, 253, 349
- Plante, S., & Sauvage, M. 2002, AJ, 124, 1995
- Popescu, C. C., & Hopp, U. 2000, A&AS, 142, 247
- Pottasch, S. R., & Bernard-Salas, J. 2006, A&A, 457, 189
- Pustilnik, S. A., et al. 2005, A&A, 442, 109
- Rosenberg, J. L., Ashby, M. L. N., Salzer, J. J., & Huang, J.-S. 2006, ApJ, 636, 742
- Rubin, R. H., et al. 2007, MNRAS, 377, 1407
- Rubin, R. H. et al. 2006, in *Galaxy Evolution Across the Hubble Time*, IAU Symposium 235, Eds. F. Combes & J. Palous, (Cambridge U. Press) (in press)
- Salzer, J. J., Jangren, A., Gronwall, C., Werk, J. K., Chomiuk, L. B., Caperton, K. A., Melbourne, J., & McKinstry, K. 2005, AJ, 130, 2584
- Searle, L., & Sargent, W. L. W. 1972, ApJ, 173, 25
- Shi, F., Kong, X., Li, C., & Cheng, F. Z. 2005, A&A, 437, 849
- Simpson, J. P., & Rubin, R. H. 1990, ApJ, 354, 165
- Simpson, J. P., Rubin, R. H., Colgan, S. W. J., Erickson, E. F., & Haas, M. R. 2004, ApJ, 611, 338
- Skillman, E. D., Kennicutt, R. C., & Hodge, P. W. 1989, ApJ, 347, 875
- Sloan, G., et al., 2007, in prep
- Smith, J. D. T., et al. 2007, ApJ, 656, 770
- Spoon, H. W. W., Marshall, J. A., Houck, J. R., Elitzur, M., Hao, L., Armus, L., Brandl, B. R., & Charmandaris, V. 2007, ApJ, 654, L49
- Stasińska, G. 2007, astro-ph/0704.0348, Lectures given at the XVIII Canary Island Winterschool “The emission line Universe”, to be published by Cambridge University Press
- Thuan, T. X., Hibbard, J. E., & Lévrier, F. 2004, AJ, 128, 617
- Thuan, T. X., Lecavelier des Etangs, A., & Izotov, Y. I. 2002, ApJ, 565, 941
- Thuan, T. X., Sauvage, M., & Madden, S. 1999, ApJ, 516, 783
- Thuan, T. X., Izotov, Y. I., & Lipovetsky, V. A. 1995, ApJ, 445, 108
- Tsamis, Y. G., & Péquignot, D. 2005, MNRAS, 364, 687
- Verma, A., Lutz, D., Sturm, E., Sternberg, A., Genzel, R., & Vacca, W. 2003, A&A, 403, 829
- Vermeij, R., Peeters, E., Tielens, A. G. G. M., & van der Hulst, J. M. 2002, A&A, 382, 1042
- Vilchez, J. M., & Pagel, B. E. J. 1988, MNRAS, 231, 257
- Werner, M., et al. 2004, ApJS, 154, 1
- Wu, Y., Charmandaris, V., Hao, L., Brandl, B. R., Bernard-Salas, J., Spoon, H. W. W., & Houck, J. R. 2006, ApJ, 639, 157
- Wu, Y., et al. 2007, ApJ, 662, 952
- Zwicky, F. 1966, ApJ, 143, 192